ELSEVIER

Surface Science 443 (1999) 31–43

surface science

www.elsevier.nl/locate/susc

Epitaxial growth of UHV magnetron sputtered Mo thin films on MgO(001) substrates, oxygen segregation and surface reconstructions

E.B. Svedberg *, [1], T.S. Jemander, N. Lin, R. Erlandsson, G. Hansson, J. Birch, J.-E. Sundgren

Department of Physics, Linköping University, S-581 83 Linköping, Sweden

Received 23 April 1999; accepted for publication 4 September 1999

Abstract

Studies of epitaxial growth of Mo thin films on MgO(001) substrates by ultrahigh vacuum (UHV) d.c. magnetron sputter deposition have shown independently by in situ low energy electron diffraction (LEED), scanning tunnelling microscopy (STM) and time-resolved in situ reflection high-energy electron diffraction (RHEED) measurements that oxygen is present on the Mo surface during the initial stages of growth. Oxygen induced reconstructions are only found for films thinner than $\sim$50 nm, and it is shown that the oxygen originates from the MgO substrate. The oxygen is causing the growing film surface to continuously reconstruct with the $(\sqrt{5}\times\sqrt{5})$R26°33′, p(2×2) and c(2×2) structures indicating O coverages ranging from $\sim$0.8–1.0 ML. STM measurements confirm earlier X-ray diffraction (XRD) and STM measurements of the $(\sqrt{5}\times\sqrt{5})$R26°33′ reconstruction and show for the first time STM images of the surface structures where p(2×2) and c(2×2) reconstructions are present. Based on our STM data we suggest surface models for the p(2×2) and c(2×2) reconstructions. The STM measurements also revealed surfaces randomly interspersed with apparent 2×2 'holes' not visible by techniques such as LEED due to their non-periodic nature.

Keywords: Molybdenum; Oxygen; RHEED; Sputtering; STM; X-ray diffraction

1. Introduction

Transition metal films, and especially molybdenum films, have recently attained considerable interest for a wide range of reasons. One application field for both molybdenum and its oxides is in the many industrial catalytic processes for oxidation, in part due to its wide range of chemical reactivity [1] but also due to the high-temperature stability of Mo. For example, the incorporation of $\sim$1 ML of oxygen atoms into the Mo surface lowers the chemical reactivity so that the normally occurring dissociation of adsorbing species, such as ammonia, is inhibited and ammonia instead adsorbs as intact molecules [2]. Molybdenum oxides have also been used for gas detectors, where detection of NO gas has been made possible [3]. Molybdenum is widely used in various thin film multilayer structures that have new and unique optical, mechanical, magnetic or electrical properties [4,5]. One usage is as sputtered thin film

* Corresponding author. Fax: +46-13-137568.

E-mail address: lynma@ifm.liu.se (E.B. Svedberg)

[1] Current address: Washington Plaza, 1420 Centre Avenue, Pittsburgh, PA 15219, USA.

0039-6028/99/$ - see front matter
PII: S0039-6028(99)00956-5

resistors on ceramic substrates where the positive temperature coefficient is an advantage as well as the extreme linearity of resistance in the -200 to $+200^{\circ}C$ range [6]. Also, Mo films have shown interesting optoelectronic properties, such as the appearance of lateral photovoltage, when layered between hydrogenated amorphous silicon layers [7]. Mo is used further as a buffer layer/substrate for epitaxial growth of other metals such as W, Nb and Ta [8].

In earlier work by Svedberg et al. [9,10] Mo has been studied as one of two constituents in different superlattice structures. It was concluded by X-ray diffraction that Mo/W superlattices exhibit an asymmetry in the interfacial intermixing due to the differences in bombarding energetic species as W vs. Mo was grown by magnetron sputtering. Furthermore, Mo/V superlattices (see Ref. [9] and references cited therein) have been investigated by reflection high-energy electron diffraction (RHEED) and transmission electron microscopy (TEM) and it was found that there exists a transition in the thickness ratio between Mo and V. At the transition the layers change their growth mode from flat to wavy, in a long distance sense, as determined by cross-sectional TEM. However, there also exist changes in the growth mode on a smaller scale where the onset of protrusions on the surface of the V layers has been detected by RHEED during growth.

In this work we have studied the initial epitaxial growth of ultrahigh vacuum (UHV) magnetron sputtered Mo films on MgO(001) substrates using techniques such as in situ low energy electron diffraction (LEED), scanning tunnelling microscopy (STM) and RHEED as well as ex situ X-ray diffraction (XRD), since the widespread use of Mo buffers calls for more detailed studies of the growth morphology and other factors affecting the desired performance of these films. For a high-temperature stable material such as Mo to be fully utilised there is a need for a matching temperature stable substrate as well, hence the choice of MgO as a substrate for the single crystalline Mo thin films. MgO has the advantage of being both stable to high temperatures and also having a suitable lattice parameter for single crystal Mo growth. The high melting point of the material, which is, application wise, a desired parameter, is also a complicating factor during the fabrication of Mo films. Mo films are not easily evaporated, instead a useful technology is sputtering which does not rely on the material melting point, and also provides acceptable deposition rates in the range of some tenths of a nanometre per second. However, with sputtering there are other factors to consider, such as the simultaneous production of high-energy backscattered gas atoms impinging on the growing film.

2. Experimental details

Mo films were deposited in two separate d.c. planar magnetron UHV sputtering systems. One of these systems is capable of in situ STM and LEED analyses and has a sputtering chamber equipped with a $180\,dm^3\,s^{-1}$ turbomolecular pump. The background pressure of the deposition chamber was always $<5\times10^{-9}$ Torr (7×10^{-7} Pa) with the substrate maintained at the deposition temperature $\sim850^{\circ}C$. The deposition chamber was connected to a UHV STM chamber, see below, making it possible to transfer the deposited films directly to the STM without breaking vacuum. One circular 22 mm planar magnetron cathode, mounted at a distance of 70 mm away from the substrate along the substrate surface normal, was used as the vapour source. The target was 99.97% pure Mo. The depositions were carried out in Ar with a purity level of 99.9999% (N60), and held at a pressure of 5.0 mTorr (0.67 Pa). The Ar pressure was monitored with a capacitance manometer. The target discharge was established using a constant power of 10 W, giving a corresponding target voltage and discharge current of ~340 V and ~0.029 A, respectively. The Mo deposition rate was $\sim0.07\,nm\,s^{-1}$ corresponding to $\sim0.4\,ML\,s^{-1}$. This deposition rate was determined by X-ray reflectivity measurements of Mo thin film samples.

The substrates used in the experiments were 0.5 mm thick $5\times10\,mm^2$, (001) oriented pre-polished MgO single crystals, from Kelpin, which were ultrasonically cleaned in successive rinses of trichloroethylene, acetone, and ethanol; dried in dry N_2; and immediately inserted in the load-lock system and transferred into the deposition chamber

to an (x, y, z, θ) substrate manipulator. Thus, the manipulator can move the sample in x, y and z directions and rotate it $>360^\circ$ so that the sample can be placed in an arbitrary position in the magnetron plasma beam. The rotation also makes it possible to start the magnetron without initiating the deposition of the sample, simply by turning the sample away from the target. Prior to initiating growth the substrates were also heat treated for 1 h at 900°C. The temperatures were determined by a calibrated IR pyrometer through a window in the chamber. Heat transfer is by conduction between the resistive heater of highly n-doped Si cut to $4\times10\times0.3\ \text{mm}^3$ and the MgO substrate ($5\times10\times0.5\ \text{mm}^3$), tapered 45° at one end. Both the heater and the MgO are clamped in place on a Mo holder with a Mo metal strip at one end, while only the Si heater is clamped at the other end. This arrangement ensures that the heater current only runs through the Si heater and not through the metal film forming during deposition. Immediately before growth the temperature was lowered to the deposition temperature and the target surface was sputter cleaned for 1 min with the MgO substrate facing away from the target.

The STM measurements were done in an in-house designed and built UHV STM [11] which is connected to the deposition chamber through a transfer chamber. The transfer chamber is pumped by a $520\ \text{dm}^3\ \text{s}^{-1}$ turbomolecular pump producing a background pressure of $<5\times10^{-11}$ Torr (7×10^{-9} Pa). In the STM chamber an ion pump ensures the background pressure is always below 1×10^{-10} Torr (1×10^{-8} Pa). The electrochemically etched W tips used are made in-house and cleaned in situ by electron bombardment heating in the UHV system. The maximum scan size is $2.6\times2.6\ \mu\text{m}^2$ and the images used throughout this project consist of 512×512 pixels.

LEED images were acquired with a VG Microtech RVL 900 rear view LEED system with three mesh optics connected to the transfer chamber. Images were taken using a 35 mm camera with a special angular preserving macro-lens for accurate image acquisition.

The second UHV system has the same base pressure but is considerably larger, compared with the deposition chamber in the first system, with a 15 times larger sample-to-wall distance. The sputtering chamber is also equipped with gas purifiers (getters) producing a 99.999999% pure Ar gas and the continuous gas throughput is much higher. The heating is by direct radiation from a BN-coated resistive graphite heater on the back side of a square $1\ \text{cm}^2$ MgO piece. Furthermore, the deposition chamber is equipped with an in situ RHEED system, from STAIB instrumente, which was used to continuously monitor the Mo film growth. The set-up will only briefly be described here, for a more extensive description see Ref. [10]. The RHEED electron-gun was operated at 35 kV and separately pumped with a $30\ \text{dm}^3\ \text{s}^{-1}$ turbomolecular pump, thus making it possible to operate it while keeping a sputtering gas pressure in the mTorr range in the chamber. The focus size of the electron beam is $<500\ \mu\text{m}$ and the divergence is 1×10^{-4} rad. Magnetic shielding, made out of μ-metal, placed inside the chamber protects the electron beam from the magnetic field generated by the magnetron sources. The shields also protect the RHEED screen from being coated during deposition. Several RHEED patterns were recorded onto videotapes, for further image processing and evaluation, with a video camera that had a resolution of 512×512 pixels and a dynamic range of 256 grey levels.

For the θ–2θ XRD measurements a Philips APD system PW 1050/25 with a repeatability of 0.01° in 2θ was utilised. For the XRD texture measurements a Philips MRD system operated with parallel beam X-ray optics and a Cu Kα radiation lab source was used, unless otherwise stated. The samples were positioned on a Eulerian cradle with 360° freedom in the azimuthal angle ϕ and 100° freedom in the tilt angle ψ which tilts the sample normal with respect to the diffraction plane, thus facilitating the collection of texture pole figures. The pole figure measurements were done with ϕ and ψ angles in the range 0–360° and 0–85°, respectively, in steps of 2°.

3. Results

To ensure comparable results, all MgO substrates were investigated prior to deposition by

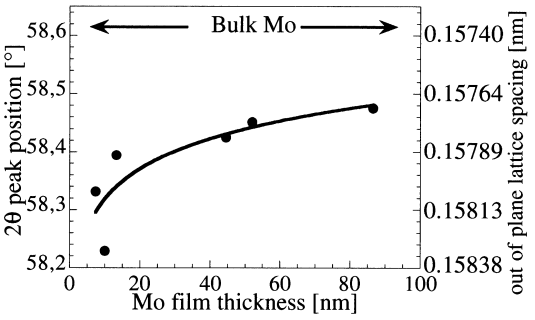

Fig. 1. Peak position of the Mo 002 XRD peak and the equivalent out-of-plane lattice spacing versus the sample thickness. The line is a guide for the eye only. Sample thicknesses ranging from 8 to 86.5 nm.

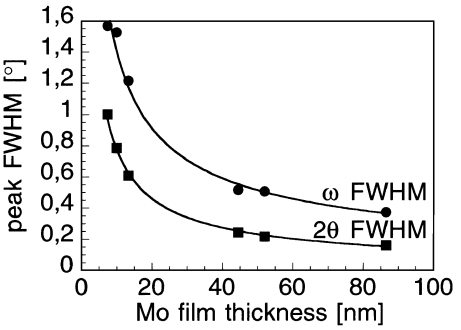

Fig. 2. The XRD ω and ω–2θ FWHM for the Mo 002 peaks versus the sample thickness. The lines are guides for the eye only.

X-ray diffraction pole figure measurements. The substrates consist of a similar set of domains with low angle grain boundaries, approximately 2°, centred around the (001) MgO substrate direction, as expected for 'high quality' commercial grade MgO substrates. The Mo films were also analysed after deposition by X-ray diffraction pole figure measurements, where the Mo(110) planes were measured, $2\theta = 40.516°$. These measurements resulted in four poles separated azimuthally 90° from each other, and tilted 45° from the surface normal of the film, thus ensuring all Mo films to be single crystalline (001) oriented Mo films with the epitaxial relationship $(001)_{Mo}/(001)_{MgO}$, $[100]_{Mo}/[110]_{MgO}$ to the MgO substrate. Most of the depositions and measurements were also performed several times with similar results to ensure reproducibility.

XRD ω–2θ measurements of the 002 Mo peak performed for samples with thicknesses ranging from 8 to 86.5 nm are presented in Fig. 1 with their peak position versus the sample thickness. As seen, the 2θ peak position shifts towards larger values with increasing film thickness so that at a thickness of 86.5 nm the 2θ value is 58.48° while it is only 58.23° at 10 nm. There is a clear trend towards increasing 2θ peak position for increased sample thickness. For the 10 nm thick sample, a peak position of $2\theta = 58.23°$ corresponds to an average out-of-plane lattice spacing of 0.1583 nm, whereas the thickest sample has an average out-of-plane lattice spacing of 0.1577 nm compared with the bulk Mo lattice parameter of 0.1574 nm. This is indicative of a relaxation away from a strained state, towards a more bulk-like Mo lattice parameter. Considering bulk lattice parameters, there would be a 5.6% compressive misfit in the plane between the MgO and Mo unit cells with the observed orientational relationship. The corresponding Scherrer coherence lengths for different Mo film thicknesses indicate that the coherence length within the film is equal to the film thickness for films up to approximately a thickness of 20 nm. For larger thicknesses the coherence length is shorter than the film thickness, indicative of crystalline defects present within the film. Measured values for the ω and 2θ full-width at half-maximum (FWHM) range from approximately 1.55 to 0.4° ω and from 1 to 0.18° 2θ, as shown in Fig. 2. In the measurements ω is the incident angle for a stationary 2θ, normally called 'rocking curve' measurements. Fig. 2 indicates that the general trend of the film crystalline quality increases with thickness, seen as a reduction in ω and 2θ FWHM values, which is also supported by a reduction of screw dislocations penetrating the surface with increasing thickness as determined by STM.

On the nanometre scale, the surface morphology is quite different for a 10 and a 50 nm thick film deposited at 870°C. Fig. 3 shows a $286 \times 286\ nm^2$ large STM image of a 10 nm thick film. As seen there is a large number of coalesced islands, $\sim 1.5 \times 10^{11}\ cm^{-2}$, with a clear tendency to align their edges in orthogonal directions. However, for the thicker films, as in Fig. 4a showing a $286 \times 286\ nm^2$ large STM image of a 50 nm thick

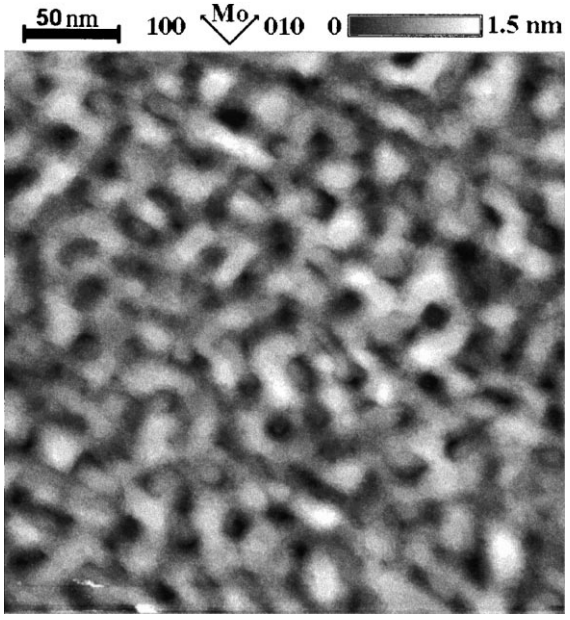

Fig. 3. STM image of a 10 nm thick Mo film grown at $T_s = 870°C$. The image size is 286×286 nm^2, z-scale is 1.5 nm from black to white, tip voltage -1.0 V and current 1.0 nA.

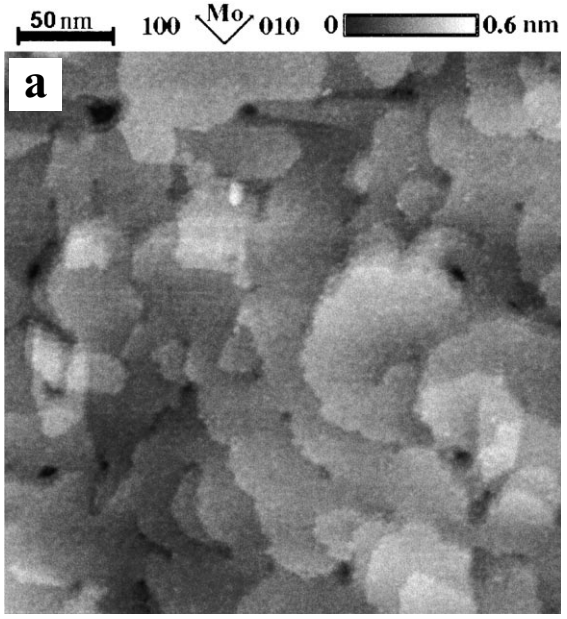

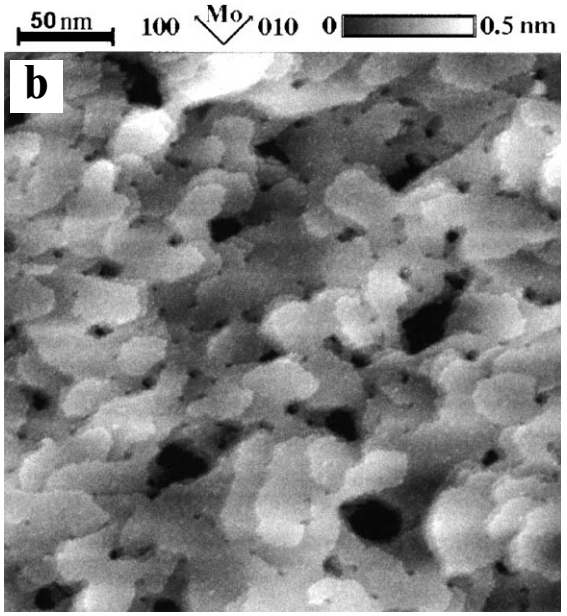

Fig. 4. (a) STM image of a 50 nm thick Mo film grown at $T_s = 870°C$. The image size is 286×286 nm^2, z-scale is 0.6 nm from black to white, tip voltage 2.3 V and current 0.9 nA. (b) STM image of a 30 nm thick Mo film grown at $T_s = 870°C$. The image size is 286×286 nm^2, z-scale is 0.5 nm from black to white, tip voltage 2.0 V and current 0.9 nA.

Mo film, there is no pronounced crystallographic orientation in the surface features, instead the surface is dominated by a high number of screw dislocations, that cause the surface to appear with a lot of 'tongues' or terraces originating at paired dislocations with left- and right-handed Burgers vectors, respectively. This gives the surface an appearance of a turbulent step-flow growth. Fig. 4b shows a 286×286 nm^2 large STM image of intermediate thickness 30 nm, the lack of pronounced crystallographic orientations in the surface features has already set in at this thickness, the surface also contains an even higher number of screw dislocations than at 50 nm.

Fig. 5a–d shows four different LEED patterns observed from the Mo surfaces at different thicknesses, ranging from ~ 8 to 50 nm, and grown at growth temperatures deviating slightly from 850°C. Fig. 5a shows a $(\sqrt{5} \times \sqrt{5})$R26°33′ LEED pattern found at 830°C during the first part of a deposition ~ 8 to 30 nm. Fig. 5b shows a c(2×2) LEED pattern that appeared at a temperature of 870°C and a Mo film thickness of ~ 8 nm. Fig. 5c shows the p(2×2) LEED pattern, measured at

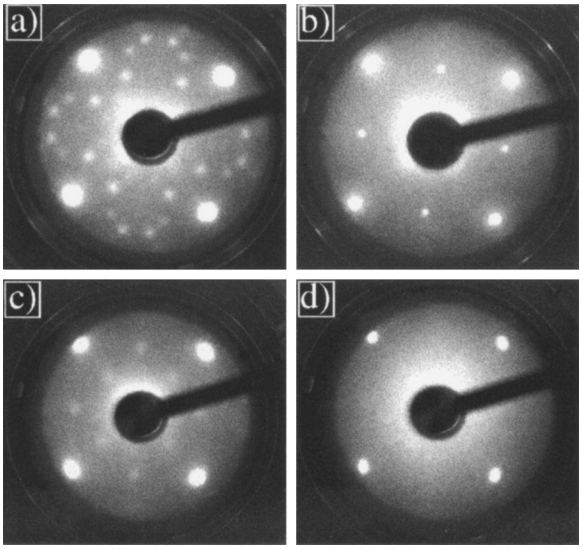

Fig. 5. Different LEED patterns, at $V_a = 46$ V, observed from the Mo surfaces at thicknesses ranging from 8 to 50 nm, and at different temperatures. (a) $(\sqrt{5}\times\sqrt{5})$R26°33′ LEED pattern from an 8 nm thick film grown at $T_s = 830$°C. (b) c(2×2) LEED pattern from an 8 nm thick film grown at $T_s = 870$°C. (c) p(2×2) LEED pattern from a 30 nm thick film grown at $T_s = 870$°C. (d) Unreconstructed (1×1) LEED pattern from a 50 nm thick film grown at $T_s = 870$°C.

Mo layer thicknesses between ~15 and 30 nm, again at a temperature of 870°C. For even thicker Mo films, ~40 to 50 nm, the reconstruction spots disappeared from the LEED pattern altogether and only the unreconstructed LEED pattern, as seen in Fig. 5d, is left over the entire surface of the sample, at temperatures of ~850°C. High magnification, atomically resolved, STM measurements of $\sim 9\times9$ nm^2 areas representative of the reconstructions observed in the LEED measurements are shown in Fig. 6. In Fig. 6a the $(\sqrt{5}\times\sqrt{5})$R26°33′ reconstruction is seen, further, Fig. 6b shows the atomic arrangement for the p(2×2) reconstruction and Fig. 6c the c(2×2) reconstruction. Apart from the surface reconstructions observed, the STM images also reveal vacancies formed in the surface. These vacancies are present both in the surface of 50 nm thick films, as well as in some thinner films, in areas where no surface reconstructions seem to exist. Further, no significant contrast effects due to variation in bias voltage were observed in the STM images. Fig. 7a

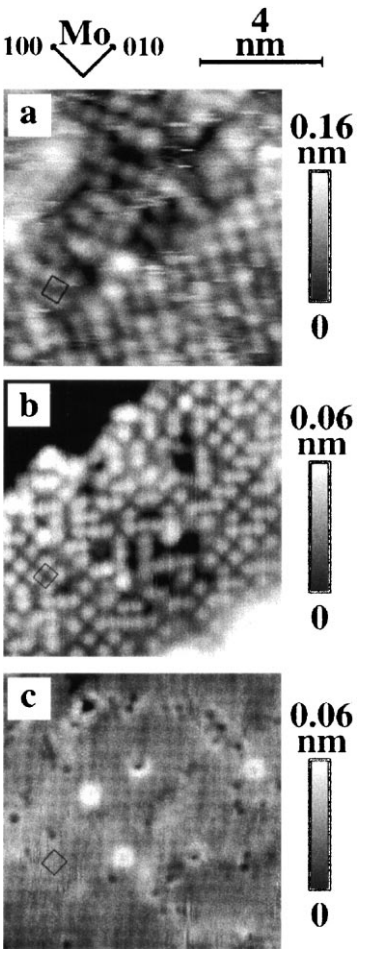

Fig. 6. Small scale, 8.94×8.94 nm^2, STM measurement, showing the atomic arrangements and unit cells of the (a) $(\sqrt{5}\times\sqrt{5})$R26°33′ reconstruction of an 8 nm thick Mo film grown at $T_s = 830$°C, z-scale is 0.16 nm from black to white, tip voltage 1.05 V and current 0.4 nA. (b) p(2×2) reconstruction of a 30 nm thick Mo film grown at $T_s = 870$°C, z-scale is 0.06 nm from black to white, tip voltage 2.3 V and current 0.9 nA. (c) c(2×2) reconstruction of an 8 nm thick Mo film grown at $T_s = 870$°C, z-scale is 0.06 nm from black to white, tip voltage 2.0 V and current 0.8 nA. Black squares represent the unit cells in each image.

is an image of a surface showing the phenomenon. Note that the vacancies are dominated by those vacancies clustered in a 2×2 form. Fig. 7b is an enlargement showing the clustered vacancies forming 2×2 'holes' in the surface.

To determine the source of the surface reconstructions, additional experiments in the second

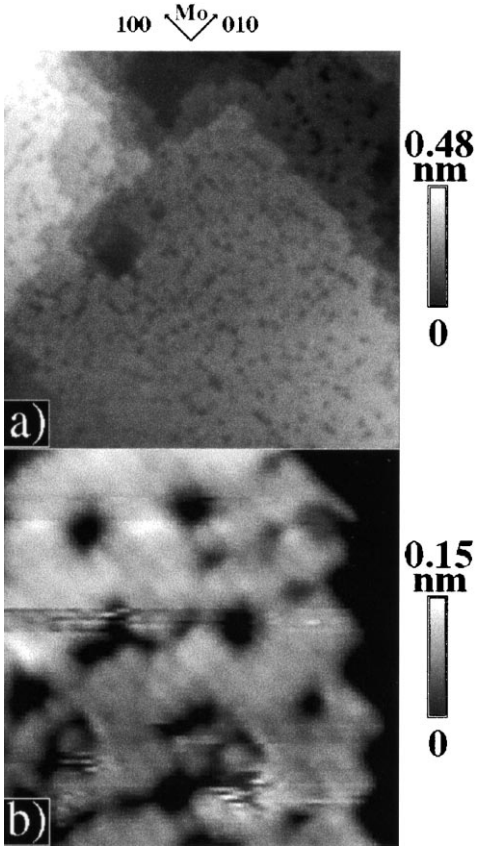

Fig. 7. STM images of a 10 nm thick Mo film grown at $T_s = 830°C$. (a) An image of the surface with size 28.4×28.4 nm^2, acquired with a z-scale of 0.48 nm from black to white, tip voltage -2.0 V and current 1.0 nA. Note that the vacancies are dominated by those vacancies clustered in a 2×2 form. (b) An enlargement with size 3.5×3.5 nm^2 showing the clustered vacancies forming the 2×2 'holes' in the surface, acquired with a z-scale of 0.15 nm from black to white, tip voltage -1.0 V and current 1.0 nA.

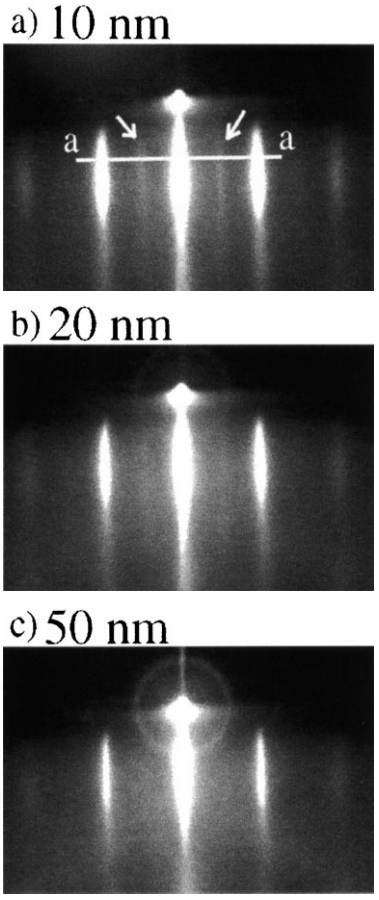

Fig. 8. RHEED pattern with electron beam parallel with the Mo [110] direction ([11] in surface mesh units) for (a) a 10 nm thick film and (b) a 20 nm thick film and finally (c) a 50 nm thick film.

UHV system equipped with a RHEED instrument were used. The zone axes during the RHEED measurements were both the Mo [100] direction ([10] in surface mesh units) as well as the Mo [110] direction ([11] in surface mesh units). Fig. 8 shows 'snap shots' from a continuous recording of the [11] pattern during the first 50 nm of growth. Half-order streaks, marked by arrows in Fig. 8a, were present in this zone axis. Along the [10] direction, not shown, there are no changes during the whole deposition of 50 nm Mo. From these experimental RHEED data at two azimuthal angles the conclusion is that during the first 20–30 nm of Mo there is a c(2×2) reconstruction present, shown schematically in Fig. 9a, while further deposition reveals no changes in the RHEED patterns along the two azimuthal directions compared with the unreconstructed Mo surface, see Fig. 9b. The evolution of the RHEED pattern along the line depicted as a–a in Fig. 8a was analysed in terms of the presence of half-order streaks. Fig. 10a shows a continuous picture of the onset and decay of the half-order streaks indicated in Fig. 8a as the film is grown. Hence, Fig. 10a is a mapping of the RHEED intensity along line a–a shown in Fig. 8a sampled every 0.2 nm during

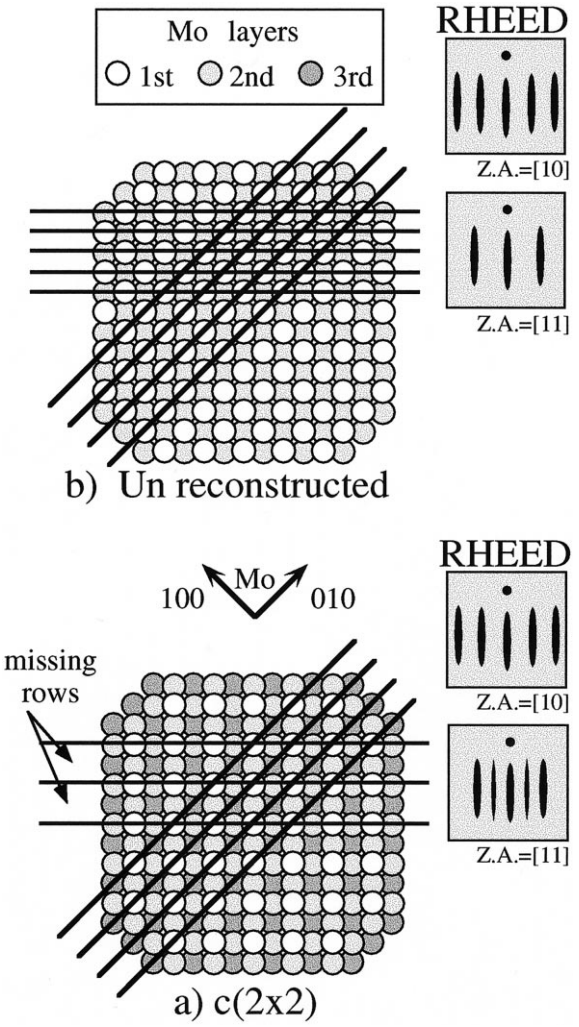

Fig. 9. Schematic representation of the Mo surface lattices and RHEED patterns, with zone axes [10] and [11], representative of (a) a c(2×2) reconstruction and (b) an unreconstructed surface.

the 50 nm thick Mo film deposition. The *y*-axis represents the position along a–a while the brightness shows the RHEED intensity for the film thickness given along the *x*-axis. Fig. 10b shows only the intensity data taken at the position for the two half-order streaks and then averaged. As seen there exist half-order streaks shortly after the deposition starts, as the initial Mo surface forms. The streaks are strongest at a film thickness of ~8 nm, whereafter they start to decay but are still

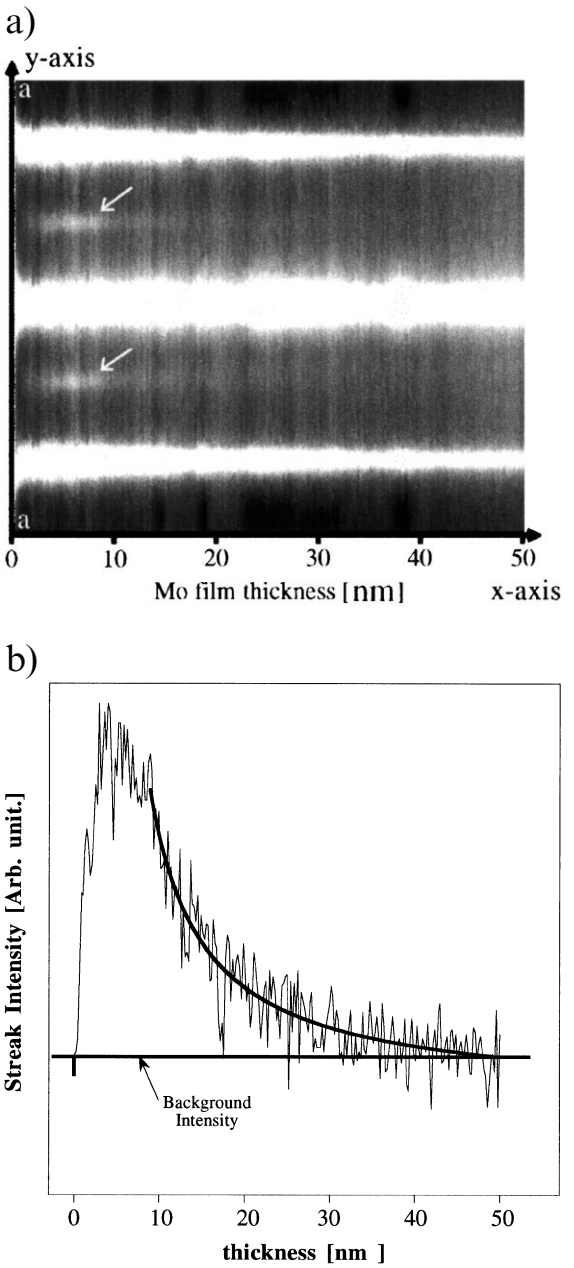

Fig. 10. (a) RHEED data acquired along the line depicted as a–a in Fig. 8a showing the evolution of the half-order streaks, as indicated by arrows, with increasing Mo film thickness. The data acquisition rate was such that the thickness increased from 0 to 50 nm in steps of 0.2 nm. (b) Intensity data taken from part a at the position for the two half-order streaks and then averaged. Background intensity level and decay of the reconstruction marked with solid lines as a guide to the eye.

visible up to ~45 nm film thickness. Further depositions of Mo on top of the initial 50 nm showed only the 1×1 pattern with no signs of reconstruction streaks.

4. Discussion

Oxygen induced reconstructions of the Mo(001) surface have been studied extensively by Bauer and Poppa [12]. At 830°C, increased oxygen coverage produces the following series of surface reconstructions: $c(4\times4)$, (2×1), $(\sqrt{5}\times\sqrt{5})R26°33'$ together with (2×1), $c(2\times2)$ and eventually faceted structures for an increased oxygen exposure. The oxygen coverage for the different ordered structures is also known from their quantitative Auger spectroscopy measurements. Of special interest here are the oxygen coverages for the $(\sqrt{5}\times\sqrt{5})R26°33'$, $p(2\times2)$ and $c(2\times2)$ structures. Bauer and Poppa observed the $(\sqrt{5}\times\sqrt{5})R26°33'$ pattern for an oxygen coverage of 0.63–0.93 ML with an especially sharp pattern in the region 0.67–0.80 ML. The $c(2\times2)$ structure was observed above 1.1 ML and up to 1.25 ML. The $c(2\times2)$ structure was also observed by Zhang et al. [13] above 0.9 ML and up to 0.98 ML at 823–1200 K. The exposure time needed to reach the lowest reported coverages, for the $(\sqrt{5}\times\sqrt{5})R26°33'$ structure, of 0.63 ML is approximately 10 min at an O_2 pressure of 2.0×10^{-9} Torr. However, neither of them reported any observations of the $p(2\times2)$ reconstruction. Observations of the $p(2\times2)$ LEED structure have, however, been made before by Ko and Madix, and their measurements indicate that the pattern is present for oxygen coverages of 1.2–1.4 ML at ~780°C [14]. Also, in a study by Overbury and Stair [15], where both the $(\sqrt{5}\times\sqrt{5})R26°33'$ and the $p(2\times2)$ reconstructions were studied, they observed the $p(2\times2)$ reconstruction for an oxygen coverage of ~0.9–1.1 ML, at a temperature of ~730°C. An overview showing the range of oxygen coverages and their corresponding reported $c(2\times2)$, $p(2\times2)$ and $(\sqrt{5}\times\sqrt{5})R26°33'$ reconstructions is given in Fig. 11.

In the literature there are no other compounds or reasons known to give the $c(2\times2)$, $p(2\times2)$ and $(\sqrt{5}\times\sqrt{5})R26°33'$ reconstructions on the Mo(100) surface other than oxygen. Hence, the observed surface reconstructions indicate the presence of oxygen on the Mo film surface. Surface oxygen can originate from several possible sources. (1) A high partial pressure of oxygen in the background gas. (2) Oxygen impurities in the Ar sputtering gas. (3) Oxygen present in the Mo sputtering target. (4) Oxygen extracted from the MgO substrate and segregating on the growth surface. (5) Ion–wall interactions during deposition causing oxygen to desorb from the walls. Results that talk against the background pressure as a possible oxygen source are, first of all, the existence of surface reconstructions only in the thin films below 30 nm thickness, even though the films deposited with larger thicknesses are flat enough to support large reconstructed surface areas. Second, repeated depositions of 50 nm Mo with minute long pauses in between each 50 nm layer show no tendency for the reconstructions to reoccur after the initial deposition that was done directly onto the MgO surface. The Ar sputtering gas or the Mo sputtering target as the oxygen source can also be ruled out by the same arguments as above. These arguments against suggestions (1)–(3) aforementioned are further supported by the fact that the time to form 2/3 ML of oxygen, i.e. what is needed to produce the $(\sqrt{5}\times\sqrt{5})R26°33'$ reconstruction, takes 10 min at an O_2 pressure of 2.0×10^{-9} Torr [12], which is also approximately the oxygen partial pressure at 5 mTorr of Ar (N60). Thus, the formation time is longer than the deposition time of the whole 8 nm thick Mo film.

The RHEED measurements in the second UHV chamber support the conclusion that the oxygen is not coming from the chamber walls or the sputtering gas. This system has about 15 times larger sample-to-wall and source-to-wall distances and is equipped with gas purifiers (getters) producing a 99.999999% pure Ar gas. As mentioned, Fig. 10 shows the decay of the half-order streaks, and thus the reconstruction during the deposition of the 50 nm Mo layer. Here, all the recorded RHEED patterns reveal that there exists oxygen shortly after the deposition starts, as determined

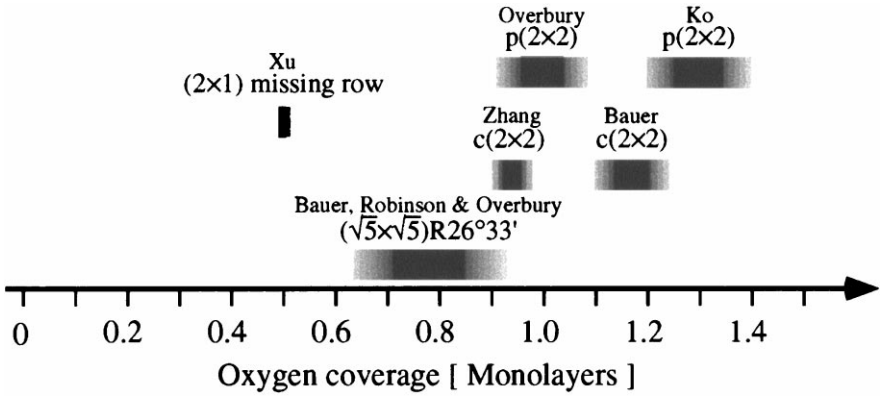

Fig. 11. Overview of the Mo surface reconstructions: $c(2\times2)$, $p(2\times2)$ and $(\sqrt{5}\times\sqrt{5})R26°33'$ as well as the (2×1) missing row reconstruction and their reported ranges from existing literature. On the *x*-axis is the oxygen coverage in monolayers as reported in each article by Bauer and Poppa [12], Zhang et al. [13], Xu and Ng [25], Robinson et al. [20], Ko and Madix [14], and Overbury and Stair [15] at a temperature of ~800°C.

from the $c(2\times2)$ reconstruction that has its strongest pattern around ~8 nm but extends up to ~30 nm where the pattern slowly fades away. Further depositions of Mo on top of the initial 50 nm induce no reconstructions.

At this stage, it is clear that possibilities (1)–(3) and (5) are eliminated as oxygen sources, and that only point (4), oxygen extracted from the MgO substrate and segregating on the growth surface, is left, for which the following reasons give further support. During the sputtering process some intermixing or atomic rearrangement, due to high energetic particle bombardment, is always present. The energetic particles are not only the sputtered Mo atoms themselves, but also backscattered energetic Ar atoms from the target. The average energy of the Ar is in the tenths of an electronvolt range, while there also exists a high energy tail extending up to some hundred electronvolts [16]. It is known that Ar^+ can sputter O from the MgO(001) surface through a momentum transfer mechanism with a threshold of ~100–140 eV, and also that Ar^{2+} causes surface O to desorb from the MgO(001) surface through an electronic process already at energies as low as ~40 eV [17]. Hence, in the initial stages of deposition there is a high possibility that there will be oxygen present in the Mo film that has its origin in the MgO crystal. The bulk diffusivity has been measured [18] for implanted oxygen in single crystalline Mo at 700°C, and a diffusion coefficient D_{bulk} of 1.0×10^{-14}–1.8×10^{-15} $cm^2\,s^{-1}$ and an activation barrier of 80.4 kJ/mol have been determined. Surface diffusivity is, however, a more complex problem, as shown by Song and Gomer [19] in their measurements of oxygen diffusivity on Mo(110) surfaces. Their results indicate considerable variations in diffusion coefficients with surface coverage, indicative of repulsive nearest-neighbour and attractive next- and next-next-nearest-neighbour oxygen–oxygen interactions. However, $D_{surface}$ is as high as $1.0\,cm^2\,s^{-1}$. Considering a simplistic Brownian motion for the bulk oxygen diffusion, the average radial distance, r, from the origin an atom has moved after t seconds is thus $r=2.4\times\sqrt{D_{bulk}\times t}$. With the lowest bulk mobility, this will be ~11 nm for a time $t=$ 119 s, which is the time needed to deposit an 8 nm thick film. Hence, it seems likely that oxygen can easily diffuse through the continuously forming Mo film and exists at the surface during the deposition.

Regarding the observed surface reconstructions, the $(\sqrt{5}\times\sqrt{5})R26°33'$ reconstruction has been investigated earlier [20] by X-ray diffraction which gives, at 0.80 ML of oxygen coverage, a surface structure with four Mo and four O atoms in a unit cell with five times the bulk 1×1 area. This structure can be viewed as a close packed array of square clusters, slightly rotated 5.5° with respect

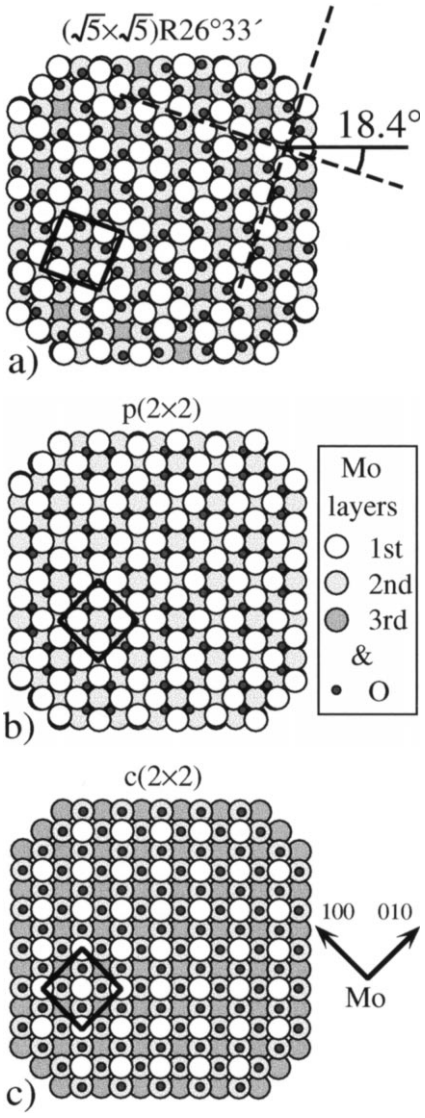

Fig. 12. Schematic model representations for the atomic arrangements of the (a) $(\sqrt{5}\times\sqrt{5})R26°33'$ reconstruction, (b) $p(2\times2)$ reconstruction and (c) $c(2\times2)$ reconstruction. Black squares represent the unit cells in each model.

to the underlying Mo unit cell, each containing a core of four Mo atoms and four O atoms decorating the edges. Fig. 12a shows a schematic image of the atomic configuration, where the arrays of square clusters can be seen forming an angle of $\sim 18.4°$ to the underlying Mo unit cell. The Mo—Mo bond length in these Mo_4O_4 clusters is 2.851 ± 0.005 Å, i.e. 9.4% shorter than in the unreconstructed surface. These data are also confirmed by STM measurements by Xu and Ng who measured a Mo—Mo bond length of 2.8 ± 0.2 Å in Mo_4O_4 clusters [21] arranged in the above predicted pattern. Our STM measurements also revealed the two surface domain orientations of the $(\sqrt{5}\times\sqrt{5})R26°33'$ structure oriented $\sim 36.9°$ $(2\times18.4°)$ relative to each other. Xu and Ng have also studied the even higher oxygen containing (2×1) surface reconstruction with STM. The results show the co-existence of $(\sqrt{5}\times\sqrt{5})R26°33'$ and (2×1) surface reconstructions on the same Mo(001) surface, and indicate a missing row (2×1) reconstruction. Fig. 6a shows different domains, where the lines of Mo_4O_4 clusters have an angle corresponding to twice the angle in Fig. 12a indicative of a $(\sqrt{5}\times\sqrt{5})R26°33'$ structure.

Taking the STM image, Fig. 6a, of the $(\sqrt{5}\times\sqrt{5})R26°33'$ surface reconstruction into consideration, as well as the proposed model for this reconstruction from the existing literature [20,21], it is possible to propose models for the $c(2\times2)$ and $p(2\times2)$ reconstructions. The STM image in Fig. 6b thus suggests an atomic arrangement for the $p(2\times2)$ surface according to the schematic representation shown in Fig. 12b, where 1 ML of oxygen is absorbed in such a way as to give the observed 2×2 clustering of the Mo atoms, seen as the white protrusions in Fig. 6b, and a larger depression in the area between four of these clusters. This arrangement of atoms and the corresponding observation by STM are marked by unit cells in both Fig. 12b and Fig. 6b, respectively. This interpretation is not in full agreement with the ion scattering simulations by Overbury and Stair [15] from which they concluded that the oxygen atoms are placed in four-fold sites on the 'unrelaxed' Mo(001) surface, and ~ 0.06 nm above it. However, they could not eliminate the possibility of a small periodic lateral displacement of the Mo layer due to the presence of oxygen, which is what is observed in Fig. 6b. Fig. 12c shows the model of the $c(2\times2)$ surface containing 1 ML of oxygen which we suggest as representative for the $c(2\times2)$ reconstruction. The model fits the expected oxygen coverage

for the reconstruction, as well as the required symmetry from the STM image shown in Fig. 6c.

Considering the aforementioned data it seems likely that at Mo film thicknesses of 8–20 nm there is a surface coverage of $\sim$0.80–1.0 ML of oxygen present, dependent on the temperature. At 50 nm thickness there is no reconstruction of the Mo film surface. The lack of reconstructions does not necessarily mean that there is no oxygen, since a rough surface morphology can inhibit the formation. However, at 50 nm there are even larger terraces present than in the case of the surface of the 8 nm thick film, indicating that the oxygen is gradually incorporated in the growing film in agreement with what can be expected for a segregating species with a non-zero incorporation probability.

Considering the thicker films of 50 nm there are no reconstructions seen in either LEED, RHEED or with STM, only 2×2 'holes', i.e. an area where there are four atoms missing in a 2×2 structure. Xu and Ng also studied the (2×1) surface reconstruction with STM. Their conclusion is that the STM data supports a missing row (2×1) reconstruction in which the atoms are placed as in Fig. 13a, i.e. the oxygen atoms are positioned in three-fold coordinated sites which are shifted off the top position on the second layer Mo atoms towards the first layer Mo atoms. Hence the Mo atoms are surrounded by oxygen atoms that seem to prevent the formation of a continuous Mo layer. From this behaviour one could speculate at a situation where the oxygen atoms occupy sites as in Fig. 13b forming 2×2 holes, as seen in the STM images in Fig. 7b. These holes may not become filled with Mo atoms for a variety of reasons, similarly to the oxygen induced (2×1) missing row reconstruction that lacks every second Mo row. The holes may induce buckling in deeper Mo layers that produces a surface of lower energy. Also the oxygen may prevent Mo atoms from occupying the empty sites and/or diffusing Mo atoms from descending step edges. It should also be pointed out that at temperatures below room temperature, both perfectly clean W and Mo(100) surfaces have a low temperature stabilised c(2×2) surface reconstruction [22,23]. This indicates an inherent tendency for the Mo(100) surface to form c(2×2) structures that might become stabilised at higher temperatures when oxygen is present.

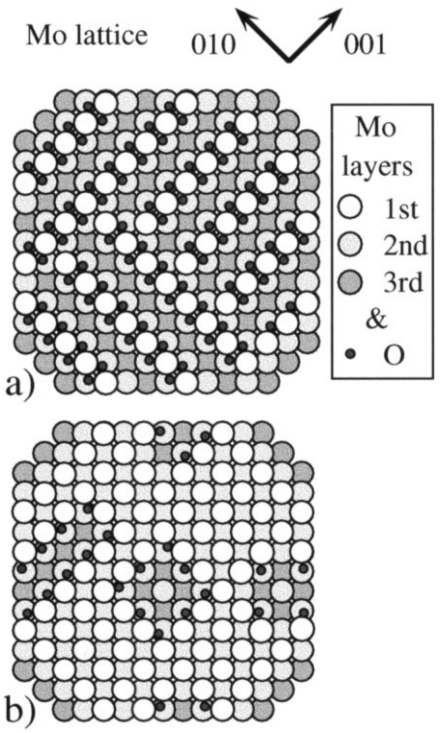

Fig. 13. Schematic model representations of the atomic arrangements of the (a) 2×1 reconstruction and (b) 2×2 holes.

However, at room temperature and above there are no surface reconstructions on the clean Mo surface [24]. One reason that these structures have not been observed before could be their non-periodic nature where they are interspersed randomly on the surface, thus, not affecting diffraction measurements such as LEED, sensitive to long-range order. If the suggestion that the oxygen inhibits the hole closure, i.e. interlayer mass transport, is correct, then the oxygen will work in opposition to a surfactant, that is intended to promote layer-by-layer growth, in the case of Mo thin film growth. Fig. 3 indicates a lack of layer-by-layer growth on the nanometre scale for the thin films where oxygen exists, while Fig. 4a shows a 50 nm thick film that has a lower oxygen coverage growing with larger flat terraces.

5. Conclusions

In summary, our results show that oxygen is present in the initial stages of Mo magnetron

sputtering deposition on MgO and that the oxygen that is apparent below a film thickness of 50 nm originates from the MgO substrate. The oxygen causes the growing film surface to reconstruct with the $(\sqrt{5}\times\sqrt{5})R26^{\circ}33'$, $p(2\times2)$ and $c(2\times2)$ structures at coverages ranging from $\sim$0.8 to 1.0 ML. STM measurements confirm earlier XRD and STM measurements of the $(\sqrt{5}\times\sqrt{5})R26^{\circ}33'$ reconstruction and show for the first time STM images of the $p(2\times2)$ and $c(2\times2)$ reconstructions, where the STM data suggest a model for the $p(2\times2)$ and $c(2\times2)$ reconstructions. At lower oxygen surface coverages, lacking evidence for reconstructions in the LEED pattern, STM measurements also reveal a surface randomly interspersed with mainly 2×2 holes. From this behaviour a geometry is suggested where, at very low oxygen coverages, the oxygen atoms occupy sites causing the formation of the 2×2 holes only visible by techniques such as STM due to their non-periodic nature.

Acknowledgements

This work was financially supported by the Strategic Research Foundation (SSF) through the Materials Research Consortium for Thin Film Growth. Valuable remarks and discussions with Professor L.D. Madsen are gratefully appreciated.

References

[1] Y. Iwasawa, Adv. Catal. 35 (1997) 187.
[2] R.M. Henry, T.A.B. Fryberger, P.C. Stair, J. Vac. Sci. Technol. 20 (1982) 818.
[3] M.D. Giulio, D. Manno, G. Micocci, A. Serra, A. Tepore, Phys. Status Solidi 168 (1998) 249.
[4] T. Tanaka, K. Kawabata, Thin Solid Films 312 (1998) 135.
[5] C. Gründling, J.A. Lercher, D.W. Goodman, Surf. Sci. 318 (1994) 97.
[6] Elektronik-Industrie 20 (1989) 80.
[7] H.-M. Lataske, T.P. Drüseday, Phys. Rev. B 58 (16) (1998) 10933.
[8] G. Mertler, M. Rey, K. Reichelt, Nucl. Instrum. Meth. 192 (1982) 535.
[9] E.B. Svedberg, Non-equilibrium surfaces of metallic thin films, Dissertation No. 549, Linköping University, Linköping, 1998.
[10] E.B. Svedberg, J. Birch, C.N.L. Edvardsson, J.-E. Sundgren, Surf. Sci. 431 (1999) 16.
[11] F. Owman, Hydrogen exposure of Si(111) surfaces and reconstructions of SiC(0001) surfaces studied with scanning tunnelling microscopy, Linköping University, Linköping, 1996, pp. 1–207.
[12] E. Bauer, H. Poppa, Surf. Sci. 88 (1979) 31.
[13] C. Zhang, M.A.V. Hove, G.A. Somorjai, Surf. Sci. 149 (1985) 326.
[14] E.I. Ko, R.J. Madix, Surf. Sci. 109 (1981) 221.
[15] S.H. Overbury, P.C. Stair, J. Vac. Sci. Technol. A 1 (1983) 1055.
[16] E.B. Svedberg, J. Birch, I. Ivanov, E.P. Münger, J.-E. Sundgren, J. Vac. Sci. Technol. A 16 (1998) 633.
[17] T. Sato, S. Takagi, T. Gotoh, Observation of sputtered ions from MgO(001) by low energy ions incident, Birmingham, 1998.
[18] V.V. Vlasov, S.S. Gerashchenko, M.I. Guseva, Atomic Energy 75 (1993) 889.
[19] Y. Song, R. Gomer, Surf. Sci. 290 (1993) 1.
[20] I.K. Robinson, D.-M. Smilgies, P.J. Eng, J. Phys.: Condens. Matter 4 (1992) 5845.
[21] H. Xu, K.Y.S. Ng, Surf. Sci. 356 (1996) 19.
[22] T.E. Felter, R.A. Baker, P.J. Estrup, Phys. Rev. Lett. 38 (1977) 1138.
[23] M.K. Debe, D.A. King, J. Phys. C: Solid State Phys. 10 (1977) L303.
[24] G.A. Somorjai, Introduction to Surface Chemistry and Catalysis, Wiley, Toronto, 1994.
[25] H. Xu, K.Y.S. Ng, Surf. Sci. 355 (1996) L305.